is 0.2 [given by the assumption (14)]. For $\lambda=800$ μ and $\lambda=2.5$ cm the maximal value of K is 0.16 and 0.014 in Si and Ge, respectively.

The numerical computations of the ratio α/K given by the formula (18) were performed for the concentrations of donors 2.0×10^{17}, 6.2×10^{17}, 2.0×10^{18} cm^{-3} in Si and 6.0×10^{15}, 1.9×10^{16}, 6.0×10^{16} cm^{-3} in Ge. At the two lower concentrations in each material we are interested in $\hbar\omega$ smaller than one-fourth of the ionization energy of a donor. We shall thus avoid the influence of the excited states of donors. At highest concentrations we are in the "intermediate region" of the impurity conduction. Apart from the problem of the conduction mechanism in this region the ground states of donors do not form yet the impurity band and our results should be valid if $\hbar\omega$ is smaller than, say, one half of the concentration-dependent activation energy ϵ_2 of conduction. We take ϵ_2 about 8×10^{-3} eV in Si (rather arbitrarily) and about 2×10^{-3} eV in Ge.[17] At still higher concentrations the ground states of donors form the impurity band and our model cannot be used. The long-wavelength limitations in our computations were given by the assumption (16) except of the highest concentration in Ge where the restriction (20) is stronger.

In the Fig. 2 we give the computed ratio α/K as a function of the wavelength of radiation for the mentioned concentrations of donors in Si and Ge. The maximal values of the absorption coefficient in our ranges of wavelength, concentration, and compensation are 190 cm^{-1} in Si ($N=2.0\times10^{18}$ cm^{-3}, $K=0.2$, $\lambda=310$ μ) and 50 cm^{-1} in Ge ($N=6.0\times10^{16}$ cm^{-3}, $K=0.2$, $\lambda=1.3\times10^{-1}$ cm).

At wavelengths larger than about 500 μ and 3×10^{-1} cm in Si and Ge, respectively, the assumption (17) is fulfilled in the whole range of integration over R in (18). For λ smaller than about 450 μ in Si and 2.5×10^{-1} cm in Ge the contribution from R's nonfulfilling (17) is about one-half of the total absorption coefficient. Thus, for such wavelengths, our results are rather semiquantitative.

ACKNOWLEDGMENTS

The authors wish to express their gratitude to Professor M. Suffczyński for many valuable remarks and discussions and to the Computing Center of the Polish Academy of Sciences for performing the numerical calculations.

[17] H. Fritzsche, Phys. Chem. Solids 6, 69 (1958).

PHYSICAL REVIEW VOLUME 136, NUMBER 1A 5 OCTOBER 1964

Phonon-Induced Relaxation in Excited Optical States of Trivalent Praseodymium in LaF_3†

W. M. YEN, W. C. SCOTT,* AND A. L. SCHAWLOW
Department of Physics, Stanford University, Stanford, California
(Received 13 May 1964)

Phonon-ion interactions have recently been shown to satisfactorily explain the temperature dependence of widths and positions of the R lines of some $3d$ ions in crystals. These interactions give rise to phonon relaxation processes and are investigated here as the mechanisms responsible for the widths and positions of sharp optical transitions in ($4f$) ions, in particular LaF_3:Pr^{3+}. The widths of transitions originating or terminating in the metastable $^3P_0$ state and involving the $^3H_4$, $^3H_6$, $^3F_2$, and $^3F_4$ states of Pr^{3+} in LaF_3 have been investigated as a function of temperature and are found to be both qualitatively and quantitatively explainable in terms of lifetime broadening of the interacting states via nonradiative processes. Temperature-dependent shifts have also been measured for the above four groups of transitions and are shown to be in qualitative agreement with theoretical predictions. Additional features of the LaF_3:Pr^{3+} spectrum, including several unreported weak transitions and vibrational sidebands, are also reported.

I. INTRODUCTION

THE thermal behavior of the widths and positions of sharp optical transitions of ($3d$) ions in solids has recently been actively investigated by a number of authors[1–10] and successfully interpreted in terms of interactions between lattice vibrations (phonons) and ions. Similar studies on ($4f$) ions in solids have been

† This work was supported by the National Aeronautics and Space Administration, under Grant NsG 331.
* National Science Foundation Predoctoral Fellow 1963–64.
[1] K. S. Gibson, Phys. Rev. 8, 38 (1916).
[2] H. K. Paetzold, Z. Physik 129, 129 (1951).
[3] A. L. Schawlow, in *Advances of Quantum Electronics*, edited by J. R. Singer (Columbia University Press, New York, 1962), p. 50; Proceedings of the Third International Conference on Quantum Electronics, 1963 (to be published).
[4] A. Kiel, Phys. Rev. 126, 1292 (1962); Johns Hopkins University Radiation Labs. Tech. Report AF-93, 1962 (unpublished).
[5] R. H. Silsbee, Phys. Rev. 128, 1726 (1962).
[6] R. J. Adler, Bull. Am. Phys. Soc. 7, 600 (1962).
[7] D. E. McCumber and M. D. Sturge, J. Appl. Phys. 34, 1682 (1963).
[8] D. E. McCumber, J. Math Phys. 5, 222 (1964); Phys. Rev. 133, A 163 (1964).
[9] G. F. Imbusch, W. M. Yen, A. L. Schawlow, D. E. McCumber, and M. D. Sturge, Phys. Rev. 133, A 1029 (1964).
[10] R. H. Silsbee and B. D. Fitchen, Rev. Mod. Phys. 36, 433 (1964).

less common,[2,3,11,12] although the optical spectra of these ions, and in particular Pr^{3+}, in hosts of different coordination have been extensively studied[13–19] and are now well understood in terms of the so-called rare-earth approximation ($V_{\text{CRYSTAL}} < V_{\text{SPIN ORBIT}}$).[20] While Dieke[11] and Kiel[4] have qualitatively discussed the general features of rare-earth ion spectral linewidths, a detailed quantitative study has not yet been undertaken.

We have investigated in detail the temperature dependence of the widths and positions of four groups (Stark manifolds) of strong optical transitions originating or terminating in the long-lived optically excited $^3P_0$ state of $LaF_3:Pr^{3+}$. We find that by generalizing the existing theory[6–9] to include these more complex spectra, we may quantitatively and qualitatively obtain an understanding of the temperature dependence of widths of rare-earth ions in solids.

In the majority of the transitions studied, even at the lowest temperatures, we find the linewidths reflect the lifetime of the interacting states, i.e., the lines are homogeneously broadened. This is, typically, not the *radiative* lifetime, but a much shorter lifetime corresponding to *nonradiative* relaxation between neighboring excited states. Since all transitions studied have the $^3P_0$ singlet in common, we may then directly compare the thermal behavior of the investigated lower Stark manifolds.

We find the linewidths of a given J manifold exhibit related temperature dependences which are characteristic to that manifold. This characteristic dependence is found to differ, markedly in some instances, among the various groups studied.

Since the crystalline structure in the neighborhood of impurity sites of LaF_3 is highly complex, a detailed analysis would be difficult. Fortunately, phonon relaxation mechanisms have characteristic and well-understood temperature dependences[21–23] which allow us to determine the dominant broadening mechanisms in each of the manifolds studied. Assuming the existence of these relaxation mechanisms, we can satisfactorily explain the thermal behavior of all the lines examined.

These same interactions are also responsible for an observable shift in the energy levels of impurity ions in crystals. In the case of the ($3d$) ions in crystals which have been studied, one observes red shifts monotonically increasing with increasing temperature, which are in excellent agreement with theoretical predictions.[7,9] In certain rare-earth cases the temperature shifts are both to the red and to the blue.[2] We propose a slight generalization of existing line shift theory[6–8] that qualitatively appears to give correct results.

Recently, the absorption and emission spectra of Pr^{3+} ions in LaF_3 have been reported.[17] We have reinvestigated in more detail the emission spectrum in the 10 000 to 22 000 cm^{-1} optical range and find excellent agreement with the published results. In addition, we have been able to detect and identify a number of hitherto unreported weak transitions.

II. EXPERIMENTAL DETAILS

Unoriented crystals of trivalent praseodymium-doped LaF_3 were kindly provided by H. Muir and R. Solomon of Varian Associates. The doping ranged from 0.1% to 10%; the majority of the work was done using crystals of 1% Pr^{3+} concentration.

Fluorescence was excited by water cooled G.E. AH–6 high-pressure mercury arc lamps. Scattering light was reduced or suppressed by using dilute $CuSO_4$ solutions and/or various combinations of glass colored filters at the source and at the entrance slits of the spectrometers used. A PEK X–76 short arc, high-pressure xenon source, passed through a Bausch and Lomb GB 89 broadband monochromator, was used to study absorption.

Spectral identification was undertaken photographically (at 77°K for convenience) using a Bausch and Lomb dual grating spectrograph. The gratings yielded dispersion figures of 8.1 Å/mm and 4.0 Å/mm, respectively. Kodak 1N and 103–0 plates were used. Exposure times ranged from a few minutes to several hours, the latter times being necessary in order to obtain weaker lines. Line positions were measured from standard reference lines superimposed on the data plates using a Grant Instrument Inc. Line Measuring Comparator. Some transitions appeared as asymmetries in other lines; these positions were obtained by manually correcting the asymmetries on graphic traces obtained using a Jarrell-Ash 23–100 recording microphotometer, or from traces obtained during linewidth measurements.

Linewidths, in absorption and fluorescence, were measured using a Jarrell-Ash 78–400, 1.8-m Ebert scanning spectrometer capable of very high resolution. Eighth or higher orders were used to match the grating blaze angle. Signals were detected by a specially housed, liquid-nitrogen cooled RCA 7265, S-20 photomultiplier. Signal-to-noise ratios were on the average better than 10:1.

[11] G. H. Dieke, in *Advances in Quantum Electronics*, edited by J. R. Singer (Columbia University Press, New York, 1962), p. 178. See also S. Yatsiv, Physica **28**, 521 (1962).
[12] W. M. Yen, A. L. Schawlow, H. Muir, and L. Mueller, Bull. Am. Phys. Soc. **8**, 231 (1963).
[13] A. M. Hellwege and K. W. Hellwege, Z. Physik **130**, 549 (1951).
[14] E. V. Sayre, K. M. Sancier, and S. Freed, J. Chem. Phys. **23**, 2060 (1951).
[15] E. V. Sayre and S. Freed, J. Chem. Phys. **23**, 2066 (1955).
[16] G. H. Dieke and R. Sarup, J. Chem. Phys. **29**, 741 (1958).
[17] E. Y. Wong, O. M. Stafsudd, and D. R. Johnston, J. Chem. Phys. **39**, 786 (1963).
[18] R. J. Elliott and K. W. H. Stevens, Proc. Roy. Soc. (London) **A215**, 437 (1952); **A218**, 553 (1953); **A219**, 387 (1953).
[19] B. R. Judd, Proc. Roy. Soc. (London) **A227**, 552 (1955); **A232**, 458 (1955).
[20] See, for example, C. J. Balhausen, *Introduction to Ligand Field Theory* (McGraw-Hill Book Company, Inc., New York, 1962); and E. U. Condon and G. H. Shortley, *Theory of Atomic Spectra* (Cambridge University Press, Cambridge, 1959).
[21] I. Waller, Z. Physik **79**, 370 (1932).
[22] J. H. Van Vleck, Phys. Rev. **57**, 426 (1940).
[23] R. de L. Kronig, Physica **6**, 33 (1939).

Temperature-dependent line shifts were measured photographically and rechecked using the scanning instrument. Line displacements were always measured from nearby standard reference lines.

Sample temperatures were controlled by direct coolants. In order to obtain intermediate temperatures, a nitrogen gas blower described elsewhere was used.[9,24] Temperatures ranged from 4.2–300°K, and were measured using thermocouples inserted in the crystals. Temperatures could easily be held to ±1°C during a measurement.

III. THEORETICAL REVIEW

The theory[4,7,25–27] of phonon-induced relaxation processes has been extensively studied[21–23,28] and has been demonstrated in ESR spin-lattice relaxation studies in rare-earth salts[25] and other paramagnetic ions and defects.[29] The theory has recently been extended to successfully explain the thermal behavior of widths and positions of sharp-line optical transitions of some ($3d$) ions in solids.[5–9] We present here a synopsis of relevant relations applying to ($4f$) ions in crystals and the manifested effects of phonon perturbations on the optical spectra of these ions in solids.

The Hamiltonian describing our system of an impurity ion in a host crystal may be written as

$$\mathcal{H}_T=\mathcal{H}_0+\mathcal{H}_p+\mathcal{H}_1, \tag{1}$$

where $\mathcal{H}_0=\mathcal{H}_{\text{FREE-ION}}+V_0$ describes the ion in the presence of a crystalline electric field V_0,

$$\mathcal{H}_p=\sum_k(a_k^\dagger a_k+\tfrac{1}{2})\hbar\omega_k$$

describes the phonon system, and

$$\mathcal{H}_1=\sum_k\left(\frac{\hbar}{2Mv^2}\right)^{1/2}C\omega_k{}^{1/2}(a_k-a_k^\dagger)$$
$$+\sum_{k,k'}\left(\frac{\hbar}{2Mv^2}\right)D\omega_k{}^{1/2}\omega_{k'}{}^{1/2}(a_k-a_k^\dagger)(a_{k'}-a_{k'}^\dagger)+\cdots$$
$$=\mathcal{H}_1'+\mathcal{H}_1''+\cdots \tag{2}$$

describes the interaction between the ion and the lattice vibrations. In these expressions, a_k and $a_k^\dagger$ are annihilation and creation operators of phonons in the kth mode, ω_k is the frequency of the kth mode, C and D are crystal-field coupling operators which operate on the electronic states $|A_i\rangle$ of the ion, M is the mass of the crystal, and v is the average sound velocity in the crystal. We have assumed throughout that $k=\omega_k/v$ and that v is independent of k.

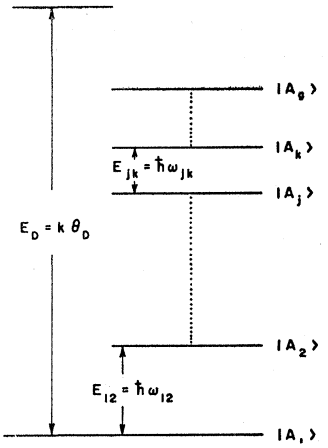

FIG. 1. Typical crystal-field splittings of rare-earth ions.

A. Linewidths of Optical Transitions

The widths of radiative transitions of ions in crystals, although they vibrate rapidly, exhibit no Doppler broadening since the amplitude of vibration is small. Moreover, radiative lifetimes of states are typically of the order of 10^{-2}–10^{-6} sec, which in terms of optical broadening may be considered negligible.[3]

Other than a few notable exceptions,[30] at the lowest temperatures the transition linewidths of ions in solids exhibit a measurable breadth which may be accounted for in some cases by random microscopic strains of the host crystal.[2,3,31,32] As temperature increases the widths invariably increase; we concern ourselves with these temperature-dependent broadening mechanisms.

Considering a system of g-electronic levels with arbitrary splitting $T_{ij}=\hbar\omega_{ij}/\kappa$, as shown in Fig. 1, for the ith level the relaxation transition probability, due to one phonon, or "direct," processes[22] is

$$W_i{}^d=\frac{2\pi}{2Mv^2\hbar}\{\sum_{j<i}\omega_{ij}\rho(\omega_{ij})|\langle A_j|C|A_i\rangle|^2[p_0(\omega_{ij})+1]$$
$$+\sum_{j>i}\omega_{ij}\rho(\omega_{ij})|\langle A_j|C|A_i\rangle|^2p_0(\omega_{ij})\}$$
$$=\pi\{\sum_{j<i}\beta_{ij}[p_0(\omega_{ij})+1]+\sum_{j>i}\beta_{ij}p_0(\omega_{ij})\}. \tag{3}$$

In Eq. (3), $\rho(\omega_{ij})$ is the detailed phonon density of states at frequency ω_{ij} and

$$p_0(\omega_{ij})=\frac{1}{\exp(T_{ij}/T)-1} \tag{4}$$

[24] W. M. Yen and R. E. Norberg, Phys. Rev. **131**, 269 (1963).
[25] P. L. Scott and C. D. Jeffries, Phys. Rev. **127**, 32 (1962).
[26] G. F. Imbusch and A. L. Schawlow (to be published).
[27] Our notation is consistent with Refs. 7 and 9. We use energy units (cm^{-1}) throughout.
[28] See, for example, R. Orbach, in *Fluctuations, Relaxation and Resonance in Magnetic Systems*, edited by D. ter Haar (Oliver and Boyd, Edinburgh, 1961), p. 219.
[29] See, for example, J. G. Castle, D. W. Feldman, P. G. Klemens, and R. A. Weeks, Phys. Rev. **130**, 577 (1963).
[30] Z. J. Kiss, Appl. Phys. Letters **2**, 61 (1963).
[31] A. A. Kaplyanskii and A. K. Przhevuskii, Dokl. Akad. Nauk SSSR **142**, 313 (1962) [English transl.: Soviet Phys.—Doklady **7**, 37 (1962)].
[32] A. L. Schawlow, A. H. Piksis, and S. Sugano, Phys. Rev. **122**, 1469 (1961).

is the thermal equilibrium phonon population of the $k(\omega_{ij})$ mode. At zero temperature, Eq. (3) becomes

$$(W_i{}^d)_0=\pi\sum_{j<i}\beta_{ij}. \tag{3a}$$

For rare-earth ions, with crystal-field separations, $\hbar\omega_{ij}$ typically of the order of 10–10^2 cm^{-1}, Eq. (3a) yields contributions to the probabilities of the order of 10^{13} sec^{-1}.[33] The latter are observable optical broadenings. The temperature dependence of the linewidth due to the direct process relaxation may be numerically evaluated and will enter solely through the phonon occupation numbers.

The emission of multiple phonons allows relaxation in cases where the splitting of electronic states is such that $T_{ij}>\theta_D$. The transition probability per unit time may be obtained by higher order perturbation theory and has been shown to be essentially temperature-independent.[4] Thus,

$$W_i{}^n\cong\sum_{j<i}K_{ij}\cong\text{constant}, \tag{5a}$$

and

$$W_i{}^2>W_i{}^3>\cdots>W_i{}^n \tag{5b}$$

where in Eq. (5b) the superscripts denote the number of phonons involved in the emission process. Multiple phonon absorption processes are negligible in the temperature ranges of interest.

Another contributing multiphonon process is the Raman process associated with phonon scattering by impurity ions; its contribution to the relaxation process may be calculated using $\mathcal{H}'$ in second order and $\mathcal{H}''$ in first; the net result for the ith level is[7]

$$\begin{aligned}W_i{}^R&=\frac{2\pi}{\hbar}\bar{\alpha}_i\left(\frac{T}{\theta_D}\right)^7\int_0^{\theta_D/T}dx\frac{x^6e^x}{(e^x-1)^2}\\&=\frac{2\pi}{\hbar}\bar{\alpha}_i\left(\frac{T}{\theta_D}\right)^7\xi_6\left(\frac{\theta_D}{T}\right),\end{aligned} \tag{6}$$

where $x=\hbar\omega/\kappa T$ and

$$\bar{\alpha}_i=\left(\frac{1}{\kappa\theta_D}\right)\left\{\alpha_i{}^2+\frac{9\hbar^2}{8\pi^4\rho^2v^{10}}\left(\frac{\kappa\theta_D}{\hbar}\right)^8\left[\sum_{j\neq i}|\langle A_j|D|A_i\rangle|^2+\sum_{i\neq j\neq k}\frac{|\langle A_j|C|A_k\rangle|^2|\langle A_k|C|A_i\rangle|^2}{E_{jk}E_{ki}}\right]\right\}, \tag{6a}$$

$$\alpha_i=\frac{3\hbar}{2\pi^2\rho v^5}\left(\frac{\kappa\theta_D}{\hbar}\right)^4\left[\langle A_i|D|A_i\rangle-\sum_k\frac{|\langle A_k|C|A_i\rangle|^2}{E_{ik}}\right]. \tag{6b}$$

In obtaining Eq. (6), we have assumed a Debye phonon density of states and have made the assumption that adjacent ionic states k are such that $E_{ik}\gg\hbar\omega$. In practice, this last assumption is not necessarily proper; resonant denominators arise if this condition is released. These terms are partially dealt with later in the development with regard to line shifts. The integral $\xi_6(\theta_D/T)$ has been tabulated by Ziman.[34]

For the ith level, the total contribution to the linewidth due to $\mathcal{H}_1$ may thus be written

$$\begin{aligned}\Delta\bar{\nu}_i&=W_i{}^d+W_i{}^n+W_i{}^R=\Delta\bar{\nu}_i{}^n+\Delta\bar{\nu}_i(T)\\&=\sum_{j<i}K_{ij}+\pi\sum_{j<i}\beta_{ij}[p_0(\omega_{ij})+1]\\&\quad+\pi\sum_{j>i}\beta_{ij}p_0(\omega_{ij})+\frac{2\pi}{\hbar}\bar{\alpha}_i\left(\frac{T}{\theta_D}\right)^7\xi_6\left(\frac{\theta_D}{T}\right).\end{aligned} \tag{7}$$

All processes in Eq. (7) give rise to a homogeneous broadening of the optical transition, and hence predict Lorentzian line shapes.[35] For any given optical transition, the Lorentzian contribution may then be expressed as the sum of the width of the transition states, i.e.,

$$\Delta\bar{\nu}_{ij}=\Delta\bar{\nu}_i+\Delta\bar{\nu}_j. \tag{7a}$$

Equation (7a) yields the temperature dependence of the homogeneous linewidth contribution due to phonon relaxation processes.

Empirically, the observed linewidth contains an inhomogeneous contribution due to random microscopic crystal strains. These strains yield a Gaussian line shape since their origin is statistical. Linewidth may be resolved into homogeneous and inhomogeneous contributions, using the numerical tables compiled by Posener.[36]

B. Line Shifts

The introduction of the perturbation $\mathcal{H}_1$ leads also to an energy level shift which may readily be evaluated; in the Debye approximation, the shift of the ith level is given by

$$\Delta E_i(T)=-\alpha_i\left(\frac{T}{\theta_D}\right)^4\int_0^{\theta_D/T}dx\frac{x^3}{e^x-1}+\frac{6}{2\pi^2\rho v^5}\sum_{j\neq i}\sum_k\frac{\omega_k{}^3}{e^x-1}\times\left\{|\langle A_j|C|A_i\rangle|^2\left[\frac{1}{E_{ij}-\hbar\omega_k}+\frac{1}{E_{ij}+\hbar\omega_k}\right]\right\},$$

when E_{ij} is in the range $\pm\hbar\omega_D$, the second term will exhibit a resonance which may be evaluated by contour integration.[7] We thus obtain

$$\begin{aligned}\Delta E_i(T)&=-\alpha_i\left(\frac{T}{\theta_D}\right)^4\int_0^{\theta_D/T}dx\frac{x^3}{e^x-1}\\&\quad+\sum_{j<i}\beta_{ij}\left(\frac{T}{T_{ij}}\right)^2P\int_0^{\theta_D/T}dx\frac{x^3}{e^x-1}\frac{1}{x^2-(T_{ij}/\theta_D)^2}\\&\quad-\sum_{j>i}\beta_{ij}\left(\frac{T}{T_{ij}}\right)^2P\int_0^{\theta_D/T}dx\frac{x^3}{e^x-1}\frac{1}{x^2-(T_{ij}/\theta_D)^2},\end{aligned} \tag{8}$$

[33] In this order of magnitude calculation, we have taken $v\sim2.5\times10^5$ cm/sec, $\theta_D\sim300°K$ and assumed $|\langle A_i|C|A_j\rangle|^2$ to be of the order of 10^3 cm^{-2} as calculated in Ref. 25.

[34] J. M. Ziman, Proc. Roy. Soc. (London) A226, 436 (1954).

[35] A. C. G. Mitchell and M. W. Zemansky, *Resonance Radiation and Excited Atoms* (Cambridge University Press, Cambridge, 1961), Chap. IV.

[36] D. W. Posener, Australian J. Phys. 12, 184 (1959).

where P denotes the principal part of the integral and α_i is given by Eq. (6b). In Eq. (8), we have neglected the phonon zero-point contribution by taking the position at 0°K as the origin. At zero temperature, the latter contribution may be non-negligible and may give rise to observable isotope shifts.[3,37]

The first term of the shift expression, Eq. (8), is, apart from a multiplicative constant, the same as the expression of the total heat of the crystal; correlation of line shift with total heat has indeed been observed.[9]

C. Vibrational Sidebands and Density of Phonon States

Again, due to the perturbation $\mathcal{H}_1$, any radiative (photon) transition between electronic levels of an ion in a crystal will exhibit emission and absorption sidebands. These sidebands correspond to the simultaneous emission or absorption of phonon-photon pairs which occur due to the mixing of state functions via the perturbation; the intensity of the sidebands may be shown to be[26]

$$I_{i\to j}\sim I_0\left[\pm\frac{\langle A_i|C|A_i\rangle}{\hbar\omega}+\sum_{j\neq i}\frac{M_{jk}}{M_{ij}}\frac{\langle A_i|C|A_k\rangle\langle A_k|C|A_j\rangle}{E_{jk}\pm\hbar\omega}\right]^2 \times[p_0(\omega)\pm 1]\omega\rho(\omega)\,, \quad (9)$$

where $M_{jk}=\langle A_k|d|A_j\rangle$ with d the appropriate dipole operator.

At zero temperature and assuming that $E_{jk}\gg\hbar\omega$, Eq. (9) reduces to

$$I_{i\to j}\sim I_0\frac{|\langle A_i|C|A_i\rangle|^2}{\hbar^2}\frac{\rho(\omega)}{\omega}; \quad (9a)$$

thus, in this approximation, the vibrational sidebands yield the allowed density of phonon states in the crystal or, more specifically, in the neighborhood of the ion site.[38]

IV. THE FLUORESCENCE SPECTRUM OF $LaF_3:Pr^{3+}$

Recently, Wong, Stafsudd, and Johnson have reported the emission spectrum of $LaF_3:Pr^{3+}$ in the 14 000 to 21 000 cm^{-1} optical range[17]; we have extended this range into the red and have been able to observe several unreported manifolds and a number of unreported lines. The unreported manifolds have been identified as $^3P_0\to{}^1G_4$, $^3F_3$ and $^1D_2\to{}^3F_2$, $^3H_6$ and $^3H_5$ transitions; the unreported lines are weak and belong to the $^3P_0\to{}^3F_4$, $^3H_6$, and $^3H_5$ transitions.

The space symmetry of LaF_3 crystals is D_{6h};[39] the ion impurity sites have been found to have C_{2v} sym-

TABLE I. Fluorescence spectrum of $LaF_3:Pr^{3+}$.[a]

λ (Å)	$\bar\nu$ (cm^{-1})	Initial state		Terminal state		I
8944.8*	11 176.6	$^3P_0$	(20 925.2)[b]	$^1G_4$	(9748.6)	3[c]
7144.3*	13 993.3	$^3P_0$	(20 925.2)	$^3F_4$	6931.9	4
7149.9	13 982.2				6943.0	2
7169.5	13 943.9				6981.3	2
7178.2*	13 927.2				6998.0	3
7194.3†	13 896.1				7029.1	1
7197.4*	13 890.1				7035.1	4
7227.4*	13 832.4				7092.8	4
7233.2†	13 821.3				7103.9	1
7264.1	13 762.5				7162.7	2
6919.3*	14 448.3	$^3P_0$	(20 925.2)	$^3F_4$	6476.9	3
6924.9*	14 436.7				6488.5	3
6928.1	14 430.0				6495.2	2
6974.0*	14 335.0				6590.2	3
7037.6*	14 207.5				6717.7	3
6331.4	15 789.7	$^3P_0$	(20 925.2)	$^3F_2$	5135.5	2
6349.8	15 744.2				5181.0	2
6357.3	15 725.6				5199.6	2
6387.8	15 650.2				5274.9	2
6390.1	15 644.9				5280.3	...
5985.3	16 703.0	$^3P_0$	(20 925.2)	$^3H_6$	4222.2	1
6000.9	16 658.4				4266.8	1
6013.7	16 624.1				4301.1	2
6044.1*	16 540.5				4384.5	3
6064.2*	16 485.6				4439.6	3
6088.2*	16 420.7				4504.5	2
6096.2*	16 399.1				4526.1	2
6106.0	16 372.8				4552.4	2
6115.7	16 346.8				4578.4	2
6120.4	16 334.3				4590.9	2
6149.6	16 256.7				4668.5	2
6189.7	16 151.4				4773.8	3
5333.0	18 746.0	$^3P_0$	(20 925.2)	$^3H_5$	2179.2	2
5367.3	18 626.2				2299.0	...
5368.9	18 620.6				2304.6	2
5370.3*	18 615.7				2309.5	4
5383.9	18 568.7				2356.5	3
5405.5*	18 491.1				2434.1	4
4777.9	20 923.8	$^3P_0$	(20 925.2)	$^3H_4$	~0	3
4791.1*	20 866.6				58.6	4
4794.9†	20 853.2				72.0	3
4809.1	20 788.1				137.1	2
4822.7†	20 729.5				195.7	2
4824.6*	20 721.3				203.9	4
4852.5†	20 602.2				323.0	2
4896.5	20 417.0				508.2	2
8501.1*	11 760.0	$^1D_2$[b]	(16 895.2)	$^3F_2$	5135.5	4
8534.3*	11 714.2		(16 895.2)		5181.0	4
8564.6*	11 672.7		(16 872.4)		5199.7	4
8594.6*	11 632.0		...		...	4
8604.4*	11 618.8		(16 895.2)		5274.9	4
8620.0*	11 597.7		(16 872.4)		5274.9	4
8624.3*	11 591.9		(16 872.4)		5280.5	3
7888.3*	12 673.5	$^1D_2$	(16 895.2)	$^3H_6$	4221.7	3
7930.0*	12 606.9		(16 872.4)		4265.5	3
7939.6*	12 591.6		(16 895.2)		4303.6	4
6659*	15 012	$^1D_2$	(17 186.5)	$^3H_5$	2174	5
6682*	14 960		...		...	5
6700*	14 921		(17 206.4)		2285	5
6721*	14 874		(17 186.5)		2312	5
6755*	14 800		...		...	5

[a] 1% Pr^{3+} in LaF_3 at 77°K.
[b] Positions obtained from Ref. 17.
[c] Arbitrary intensity scale, 1 denotes very strong line, 5 denotes very weak line.
* Not reported in Ref. 17.
† Line asymmetric.

[37] G. F. Imbusch, W. M. Yen, A. L. Schawlow, G. E. Devlin, and J. P. Remeika, Phys. Rev. (to be published).
[38] E. W. Montroll and R. B. Potts, Phys. Rev. 100, 525 (1955).
[39] R. W. G. Wyckoff, *Crystal Structures* (Interscience Publishers, Inc., New York, 1951), Vol. II.

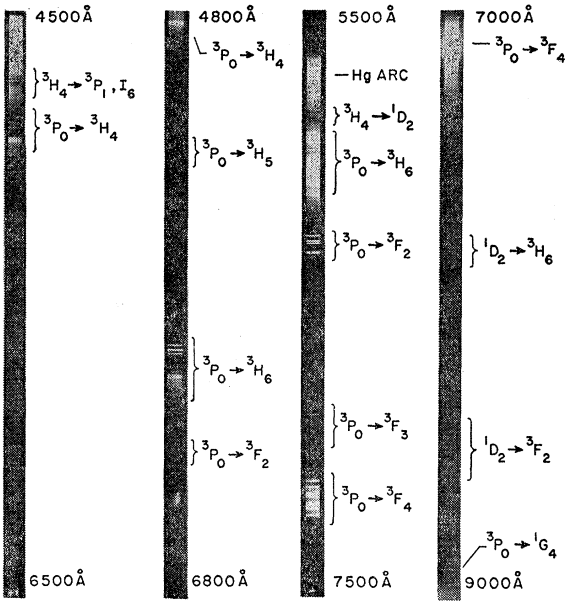

FIG. 2. Optical spectrum of 1% LaF_3:Pr^{3+} at 77°K. Transitions involved are as shown; very sharp lines are gas discharge references.

metry which can be considered as distorted D_{3v}.[40–42] For non-Kramers ions, C_{2v} symmetry will in general lift all degeneracy in a given J state, i.e., each weak crystal-field J state will split into $2J+1$ nondegenerate levels. Radiative transitions in this coordination are all electric dipole transitions, since no inversion symmetry exists about the ion site. The selection rules are easily worked out.[20]

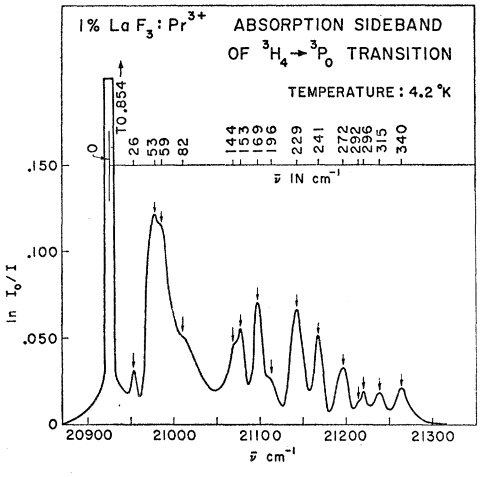

FIG. 3. Absorption sideband of $^3H_4 \rightarrow {}^3P_0$ transition of 1% LaF_3:Pr^{3+} at 4.2°K. Distance of sideband peaks from the "no-phonon" 4778 Å line are shown on upper scale.

[40] I. Oftedal, Z. Physik. Chem. **6**, 272 (1929); **13**, 190 (1931).
[41] D. A. Jones, J. M. Baker, and D. F. D. Pope, Proc. Phys. Soc. (London) **74**, 249 (1959).
[42] E. Y. Wong, O. M. Stafsudd, and D. R. Johnston, Phys. Rev. **131**, 990 (1963).

The fluorescence of LaF_3:Pr^{3+} originates primarily from the singlet $^3P_0$ level which is 20 925 cm^{-1} above the lowest crystal state of the $^3H_4$ ground-state manifold. Relatively weak emission is also observed from the $^1D_2$ level, but no emission originates from $^3P_1$ or higher levels. The observed emission spectrum in the 10 000 to 21 000 cm^{-1} region is summarized in Table I. The energy level assignment is in very good agreement with that of Wong and co-workers.[17] The lines marked with asterisks (*) in the $^3P_0 \rightarrow {}^3F_4$, $^3H_6$, and $^3H_4$ manifolds of Table I were weak lines unreported in the reference and apparently correspond to first-order forbidden transitions and which can occur through slight distortions or imperfections in the ion site symmetry. Figure 2 shows the emission spectrum of LaF_3:Pr^{3+} at 77°K.

We have observed vibrational sidebands of the various fluorescence and absorption manifolds. At 4.2°K, as expected, emission sidebands appear to the red or less energetic side of the parent pure electronic

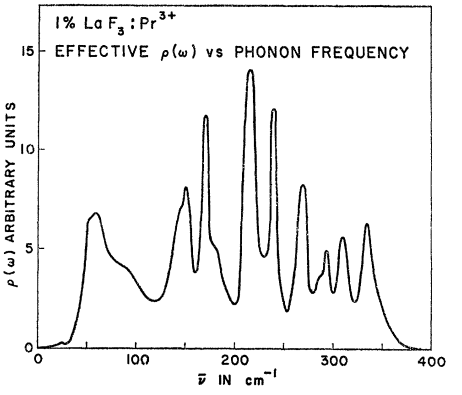

FIG. 4. "Effective density of phonon states" $\rho(\omega)$ of LaF_3:Pr^{3+} approximated from Eq. (9a).

transition whereas the absorption sidebands appear to the blue of the parent line. Since each sharp line electronic transition is accompanied by such sidebands, observed sidebands of a given Stark manifold are greatly complicated by overlap. The simplest transition is the $^3H_4 \rightarrow {}^3P_0$ absorption singlet at low temperatures; the observed sideband of this transition is shown in Fig. 3. The various prominent peaks that appear in the figure are probably frequencies corresponding to the normal modes of the impurity site unit cell.[43,44] In the approximation of Eq. (9a), we obtain the effective density of state which is shown in Fig. 4, and which we will use throughout.

Figure 5 shows the emission sideband of the $^3P_0 \rightarrow {}^3F_2$ transition; some of the frequencies appearing in Fig. 3 appear to be identifiable in this sideband. A detailed analysis of the sideband structure is not undertaken in

[43] I. Richman, R. A. Satten, and E. Y. Wong, J. Chem. Phys. **39**, 18 (1963).
[44] I. Richman, Phys. Rev. **133**, A 1364 (1964).

this paper since the low site symmetry makes normal-mode analysis very difficult. Using Fig. 14, however, we may make an estimate of the Debye temperature of LaF_3 by averaging over the structure and approximating the total area by a smooth Debye curve. This procedure yields a value

$$\theta_D = 360°\mathrm{K}, \tag{10}$$

which is consistent with previously reported values[12] and with the general bulk elastic properties of the lattice.[45]

V. RESULTS AND INTERPRETATION

A. Line Shapes and Widths at 4.2°K

In this section we discuss the observed low-temperature line shapes of four groups of radiative transitions originating or terminating on the singlet $^3P_0$ state of

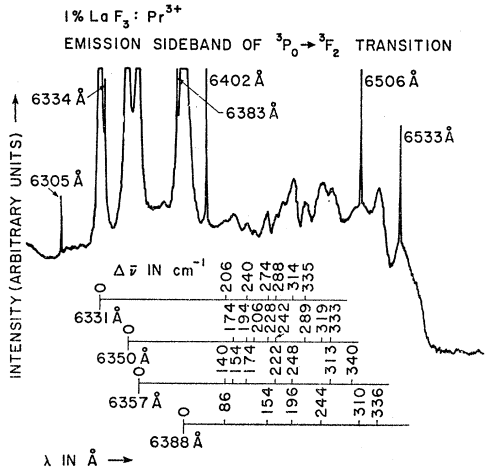

FIG. 5. Vibrational sideband of $^3P_0 \rightarrow {}^3F_2$ transition at 77°K. Sharp lines are Ne reference lines; vibrational peak distances from various "no-phonon" lines are shown in lower scale.

LaF_3:Pr^{3+}. In particular, we discuss the strong fluorescences to the $^3F_4$, $^3F_2$, $^3H_6$, and $^3H_4$ Stark levels and the $^3H_4 \rightarrow {}^3P_0$ absorption which is a singlet at low temperatures.

The $^3P_0$ state is a metastable state with a radiative lifetime of $\sim 100\ \mu$sec[46]; the state is thermally broadened solely through a modulation via lattice phonons. This modulation is just the Raman process discussed in Sec. III.[3] The homogeneous width of the $^3P_0$ state may then be described as

$$\Delta\bar{\nu}(^3P_0) = \bar{\alpha}(^3P_0)(T/\theta_D)^7 \xi_6(\theta_D/T), \tag{11}$$

[45] This procedure is in complete analogy to that used in Cr^{3+} and V^{2+} studies (Refs. 7 and 9). In the latter an "effective or reduced" Debye temperature is used; lack of specific data on the LaF_3 lattice prevents us from following the latter procedure. Conversely, the actual Debye temperature should be larger than our estimated values.

[46] R. Solomon (private communication).

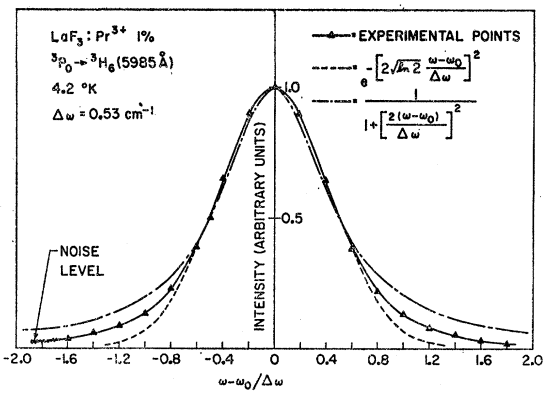

FIG. 6. Low-temperature line shape of 5985 Å line shown against normalized Gaussian and Lorentzian shapes.

where

$$\bar{\alpha}(^3P_0) = \frac{9}{4\pi^3\rho^2 v^{10}}\left(\frac{\kappa\theta_D}{\hbar}\right)^7 \times\{2\langle {}^3P_0|D|{}^3P_0\rangle + \sum_j{}' |\langle A_j|D|{}^3P_0\rangle|^2\}, \tag{11a}$$

and $\sum'$ is the sum over all other electronic states $j \neq {}^3P_0$.

At low temperatures, the width of the $^3P_0$ state may, thus, be considered negligible and Eq. (7a) reduces to

$$\Delta\bar{\nu}_{ij} = \Delta\bar{\nu}_i.$$

We then may expect to observe the homogeneous contribution of the terminal (or originating) state in a fluorescence (or absorption) transition involving the $^3P_0$ state if the strain contributions are such that

$$\Delta\bar{\nu}_{ij}{}^{\mathrm{STRAIN}} \lesssim \Delta\bar{\nu}_i.$$

We find that all lines investigated, with the exception of the low-temperature 5985 Å$(^3P_0 \rightarrow (^3H_6)_1)$ and 4778 Å$((^3H_4)_1 \rightarrow {}^3P_0)$ lines, show Lorentzian shapes to within experimental error (Figs. 6 and 7). The two

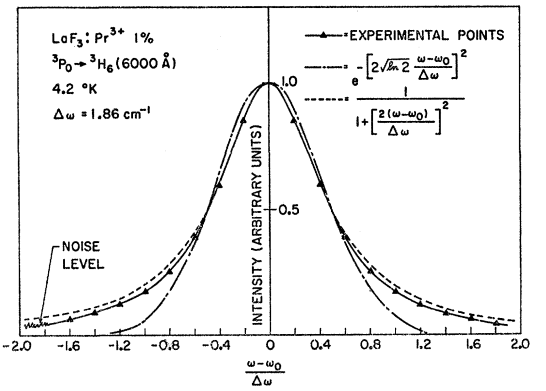

FIG. 7. Low-temperature line shape of 6000 Å line shown against normalized Gaussian and Lorentzian shapes. The slight wing deviations may be corrected by substracting the strain width.

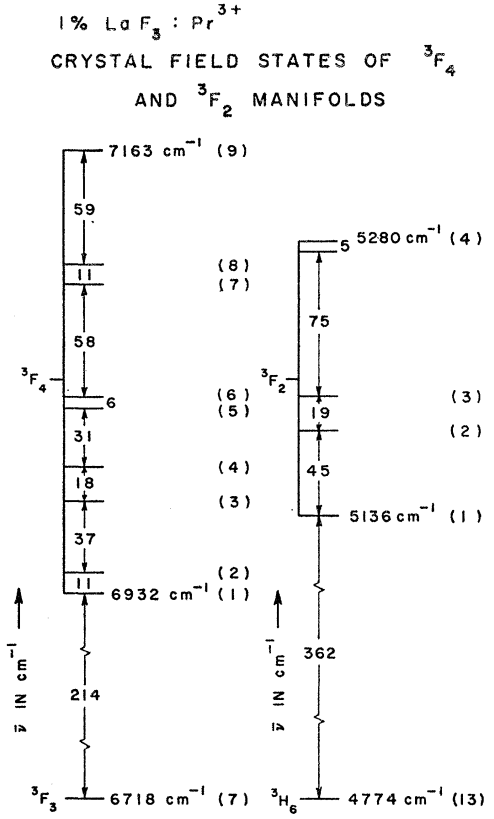

FIG. 8. Schematic energy level diagram of the $^3F_4$ and $^3F_2$ manifolds of LaF_3:Pr^{3+} showing nearest adjacent crystal-field states.

exceptions show line shapes that approximate Gaussians, indicating that the levels are being inhomogeneously broadened. The 5985 Å line of LaF_3:Pr^{3+} at 4.2°K is shown in Fig. 6[47]; the profile follows a Gaussian closely at the center and shows slight deviations at the wings. Such deviations have been observed and reported for the 4.2°K R lines of MgO:Cr^{3+} and V^{2+} and are likely to be caused by macroscopic crystal strains.[9] The strain width is such that

$$(\Delta\bar{\nu})_{4778}{}^{\text{STRAIN}}=(\Delta\bar{\nu})_{5985}{}^{\text{STRAIN}}=0.53\ \text{cm}^{-1}. \quad (12)$$

We make the assumption that the strain width is a constant for all observed transitions, and that it is independent of temperature. Neither one of these assumptions is rigorously justifiable; however, the error introduced by making such assumptions is probably small.[9]

Figure 7 shows the 6000 Å ($^3P_0\rightarrow(^3H_6)_2$) line in profile. The contour follows a Lorentzian far into the wings indicating that it is lifetime limited; as we shall see in the next subsection, we can attribute this lifetime to relaxation to the $(^3H_6)_1$ state via spontaneous emission of phonons.

The measured widths, at 4.2°K, having been corrected for the strain width, yield from Eq. (7) the spontaneous emission coefficients of single or multiple phonons, i.e., $\sum_{j<i}\beta_{ij}$ and $\sum_{j<i}K_{ij}$. These values are used in obtaining quantitative predictions for the thermal dependence of linewidths.

The dominant inter-Stark manifold relaxation mechanism may be determined by considering the 4.2°K widths of the lowest energy state of each manifold. The schematic energy level diagrams of the manifolds studied are shown in Figs. 8 and 9; for the excited manifolds $^3F_4$, $^3F_2$, and $^3H_6$, we observe the strain corrected values to follow the relation

$$\Delta\bar{\nu}(^3F_4)_1=7.20\ \text{cm}^{-1}>\Delta\bar{\nu}(^3F_2)_1=2.16\ \text{cm}^{-1}\gg\Delta\bar{\nu}(^3H_6)_1\simeq 0. \quad (13)$$

Equation (13) may easily be understood, for the lifetime of the lowest state of each manifold depends on the energy separation to the next lowest crystal-field level. From Figs. 8 and 9 for the $(^3F_4)$ states $E(^3F_4)_1-E(^3F_4)_7\lesssim\kappa\theta_D$, and relaxation may occur via the direct process, whereas ions in the $^3F_2$ and $^3H_6$ states must emit two

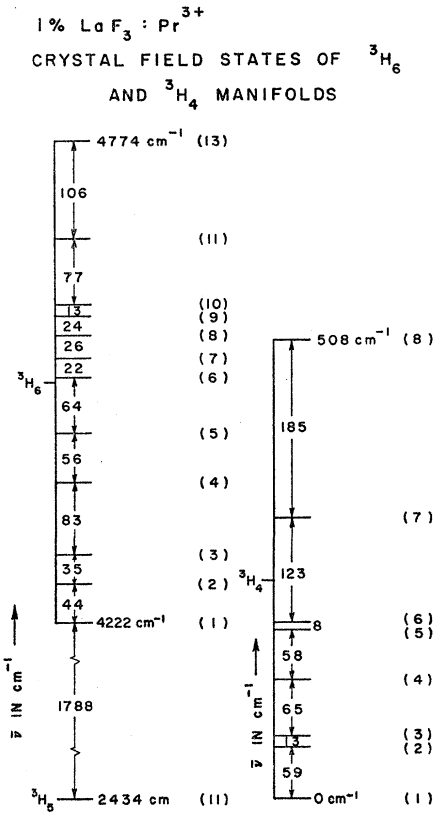

FIG. 9. Schematic energy level diagram of the $^3H_6$ and $^3H_4$ manifold. Levels $(^3H_6)_{12}$ and $(^3H_4)_9$ were not assigned.

[47] There is additional interest in this line since it recently has been reported to exhibit stimulated emission. R. Solomon and L. Mueller, Appl. Phys. Letters 3, 135 (1963).

and n phonons, respectively, in order to relax since

$$E(^3F_2)_1 - E(^3H_6)_{13} \gtrsim \kappa\theta_D$$

and

$$E(^3H_6)_1 - E(^3H_5)_{11} \gg \kappa\theta_D .$$

Thus, from Eq. (5b), the low-temperature widths should indeed follow the condition

$$\Delta\bar{\nu}(^3F_4)_1 > \Delta\bar{\nu}(^3F_2)_1 \gg \Delta\bar{\nu}(^3H_6)_1 , \qquad (13a)$$

and we may conclude that the dominant inter-manifold relaxation mechanism is a one-phonon process for the $(^3F_4)$ states, a two-phonon process for the $(^3F_2)$ states, and a n-phonon process for the $(^3H_6)$ states.

The $(^3H_6)_1$ state is the terminal state of the 5985 Å fluorescence line discussed previously and shown in Fig. 6. The strain width completely masked the homogeneous contribution of this level indicating that it is probably metastable and that there is a possibility that this level may relax via a radiative transition.

B. Linewidths and Temperature Dependence

We now discuss the observed temperature dependence of the linewidths of some of the strongest radiative transitions involving the singlet $^3P_0$ state. The experimental results and identification of the transitions studied are shown in Figs. 10, 11, 12, and 13. All linewidths have been corrected for strain taking $\Delta\bar{\nu}^{\text{STRAIN}} = 0.53\ \text{cm}^{-1}$ and using the numerical results of Posener.[36]

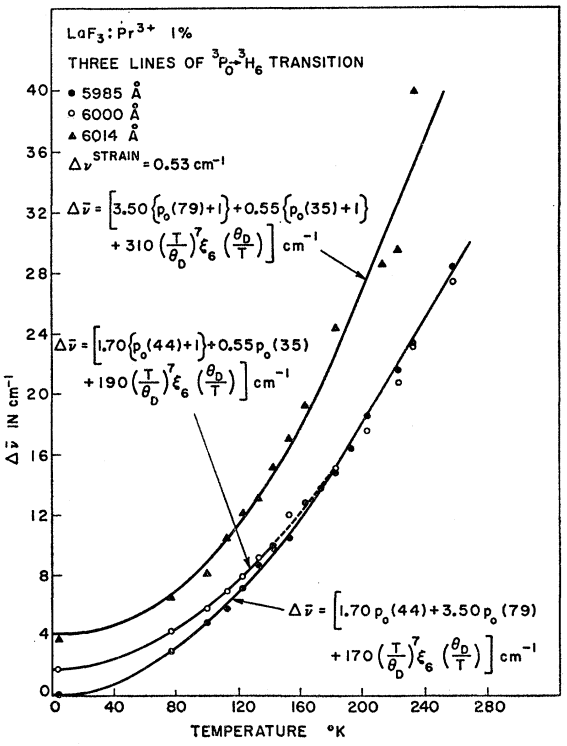

FIG. 10. Temperature dependence of the linewidths of three strong lines of the $^3P_0 \rightarrow {}^3H_6$ transition. Solid lines are calculated values of the functions shown in diagram. Error bars on experimental points are ±10%.

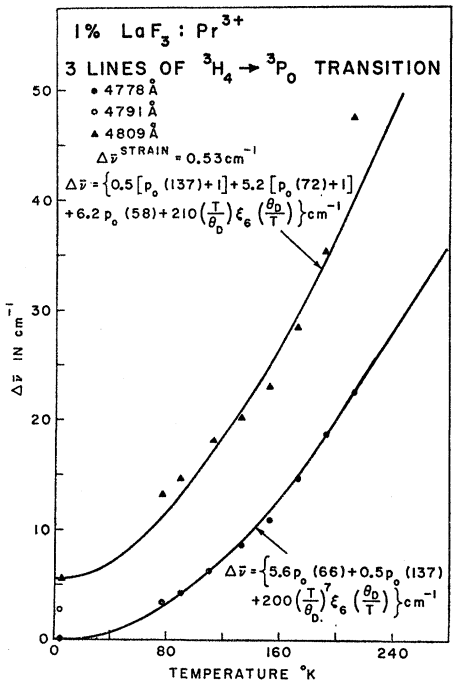

FIG. 11. Temperature dependence of the linewidths of three strong lines of the $^3H_4 \rightarrow {}^3P_0$ transition. The 4791 Å was not investigated except at 4.2°K (see text).

As expected, all widths increase as temperature increases; we note, further, that the widths of a given manifold exhibit characteristic and similar temperature dependences. This dependence varies among the groups studied. For example, the widths of the $^3H_4$ states increase 30–50 cm^{-1} in going from 0–300°K, whereas the $^3F_2$ widths increase by only 5–10 cm^{-1} over the same range.

Referring to the schematic energy level diagrams (Figs. 8 and 9) and assuming the temperature dependences of phonon relaxation processes of Sec. III, we can quantitatively explain the thermal behavior of the linewidths studied. In the following section, we discuss the results of one set of transitions in detail to illustrate our procedure.

(i) *The $^3H_6$ Manifold*

The temperature dependence of the linewidths of the $^3P_0 \rightarrow (^3H_6)_{1,2,3}$ transitions is shown in Fig. 10. The widths in the 0–300°K temperature range may be well described by relations of the type given by Eq. (7).

For the levels of the $^3H_6$ manifold with $\sum_{j<i} K_{ij} \cong 0$, Eq. (7a) reduces to

$$\Delta\bar{\nu}_i + \Delta\bar{\nu}(^3P_0) = \pi \sum_{j<i} \beta_{ij}[p_0(\omega_{ij},T)+1] + \pi \sum_{j>i} \beta_{ij} p_0(\omega_{ij},T) + \alpha_i (T/\theta_D)^7 \xi_6(\theta_D/T) , \qquad (14)$$

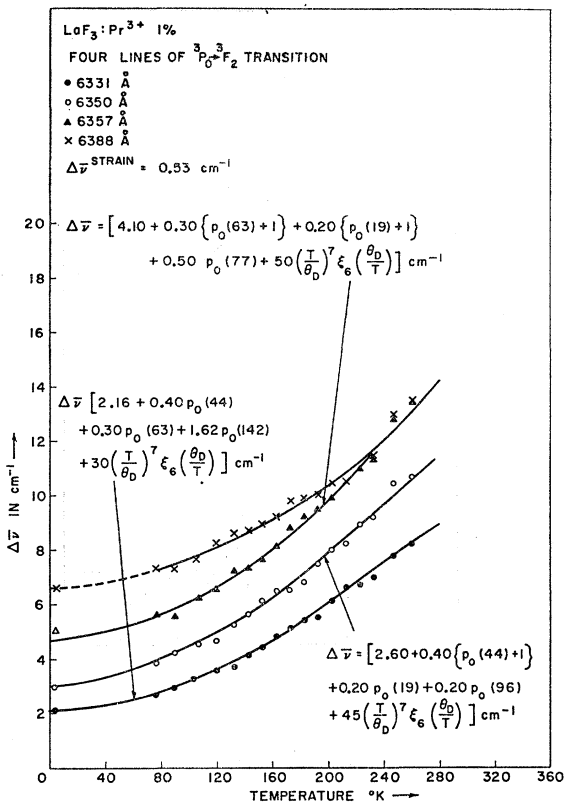

FIG. 12. Temperature dependence of the linewidths of four strong lines of the $^3P_0 \rightarrow {}^3F_2$ transition. The 6388 Å line was not fitted.

where $\Delta\bar{\nu}(^3P_0)$ is given by Eq. (11). For simplicity in fitting all our linewidth results, we have neglected single-phonon absorption processes involving the $(^3H_6)_4$ and higher levels. For these levels, in the temperature ranges studied, the neglect of these processes will introduce errors less than our experimental accuracy of $\pm 10\%$.

From Eq. (3), it is clear that

$$\beta_{ij} \equiv \beta_{ji}; \tag{15}$$

thus, for the three levels of the $^3H_6$ manifold studied, the following six coefficients remain to be determined from our data: $\beta_{12}, \beta_{13}, \beta_{23}, \bar{\alpha}_1, \bar{\alpha}_2, \bar{\alpha}_3$.

From the previous sections, we note that the 0°K intercept of the linewidth curves yields

$$\Delta\bar{\nu}_2 = \pi\beta_{21} = \pi\beta_{12}, \tag{16}$$

and

$$\Delta\bar{\nu}_3 = \pi(\beta_{31}+\beta_{32}) = \pi(\beta_{13}+\beta_{23}). \tag{17}$$

Equations (16) and (17) then reduce the undetermined parameters to four.

For level $(^3H_6)_1$, with β_{12} determined by Eq. (16), we require a two-parameter fit to account for the temperature dependence of the linewidths, i.e., we need to determine β_{13} and $\bar{\alpha}_1$. The determination of these two coefficients may be carried out quite accurately, since the functional temperature dependence of the direct and Raman processes differ dramatically. Once β_{13} is determined, β_{23} is uniquely determined through Eq. (17); the widths of $(^3H_6)_2$ and $(^3H_6)_3$ each then contain one undetermined coefficient, i.e., $\bar{\alpha}_2$ and $\bar{\alpha}_3$, respectively, since all direct process coefficients β_{ij} have been fixed. Thus, the determination of the coefficients is not as arbitrary as it might seem at first glance, on the contrary, the self-consistency required by equations of the type Eqs. (15), (16), and (17) and the experimental results serve to overdetermine the fitting process.

We find for three lines studied, the temperature dependence of the linewidths is describable by

$$\Delta\bar{\nu}_1 = \{1.70p_0(44,T) + 3.50p_0(79,T) + 170(T/\theta_D)^7\xi_6(\theta_D/T)\}\text{cm}^{-1} - \Delta\bar{\nu}(^3P_0), \tag{18a}$$

$$\Delta\bar{\nu}_2 = \{1.70[p_0(44,T)+1] + 0.55p_0(35,T) + 190(T/\theta_D)^7\xi_6(\theta_D/T)\}\text{cm}^{-1} - \Delta\bar{\nu}(^3P_0), \tag{18b}$$

$$\Delta\bar{\nu}_3 = \{3.50[p_0(79,T)+1] + 0.55[p_0(35,T)+1] + 310(T/\theta_D)^7\xi_6(\theta_D/T)\}\text{cm}^{-1} - \Delta\bar{\nu}(^3P_0). \tag{18c}$$

The splittings involved in $p_0(\omega_{ij},T)$ are in reference to Fig. 9, and $\pi\beta_{12} = 1.70$ cm^{-1}, $\pi\beta_{13} = 3.50$ cm^{-1}, and $\pi\beta_{23} = 0.55$ cm^{-1} satisfy Eqs. (16) and (17) to within experimental accuracy.

The calculated values of $\Delta\bar{\nu}_i + \Delta\bar{\nu}(^3P_0)$ given by Eqs. (18a)–(18c) are plotted as solid lines in Fig. 10. The agreement with the experimental results is well within the experimental uncertainty of $\pm 10\%$.

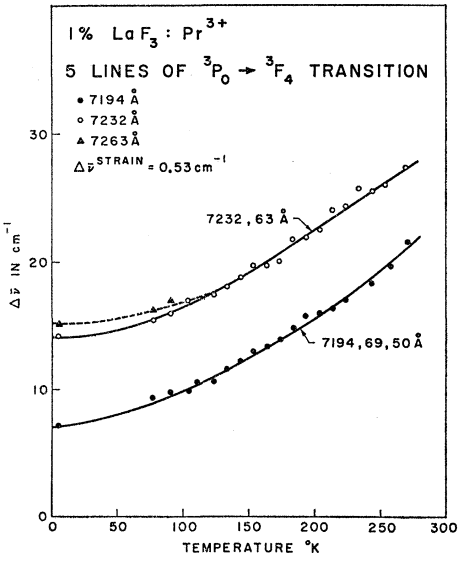

FIG. 13. Temperature dependence of the linewidths of five lines of the $^3P_0 \rightarrow {}^3F_4$ transition. Solid lines are best fit curves. The experimental values of the 7169 and 7150 Å followed the values of the 7194 Å closely and were not plotted.

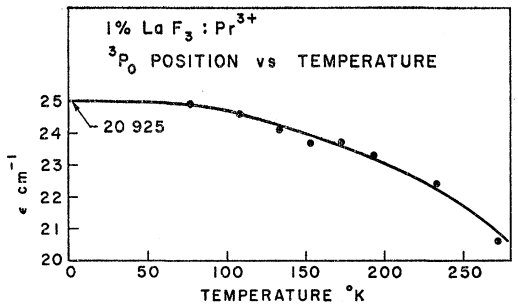

FIG. 14. Position of the $^3P_0$ state versus temperature (see text).

(ii) The $^3H_4$ Manifold

The majority of the linewidths involving this manifold were taken in absorption. We find, using the procedure already described, that for the two lines studied the temperature dependence of the linewidths is describable by

$$\Delta\bar{\nu}_1=\{5.60p_0(66,T)+0.50p_0(137,T)+200(T/\theta_D)^7\xi_6(\theta_D/T)\}\text{cm}^{-1}-\Delta\bar{\nu}(^3P_0) \quad (19a)$$

and

$$\Delta\bar{\nu}_4=\{0.50[p_0(137,T)+1]+5.20[p_0(72,T)+1]+6.20p_0(58,T)+210(T/\theta_D)^7\xi_6(\theta_D/T)\}\text{cm}^{-1}-\Delta\bar{\nu}(^3P_0). \quad (19b)$$

Results are shown in Fig. 11, the solid lines again being calculated values of Eqs. (19a) and (19b).

Referring to the energy level diagram of $^3H_4$ (Fig. 9), the above two relations were fitted by considering the center of gravity of the 2nd and 3rd levels, the error introduced in this manner is within our experimental accuracy. Even at 77°K, the two levels could not be clearly resolved in absorption and the lines showed unaccountable complicated structure. The single point in Fig. 11 involving the $(^3H_4)_2$ level, i.e., the 4971 Å line, was measured in fluorescence at 4.2°K; the corresponding low-temperature transition involving the $(^3H_4)_3$ level is weak and no width measurements were attempted.

(iii) The $^3F_2$ and $^3F_4$ Manifolds

For the $^3P_0\rightarrow{}^3F_2$ transitions (Fig. 12), we find the widths to be describable by

$$\Delta\bar{\nu}_1=\{2.16+0.40p_0(44,T)+0.30p_0(63,T)+1.62p_0(142,T)+30(T/\theta_D)^7\xi_6(\theta_D/T)\}\text{cm}^{-1}-\Delta\bar{\nu}(^3P_0), \quad (20a)$$

$$\Delta\bar{\nu}_2=\{2.60+0.40[p_0(44,T)+1]+0.20p_0(19,T)+0.20p_0(96,T)+45(T/\theta_D)^7\xi_6(\theta_D/T)\}\text{cm}^{-1}-\Delta\bar{\nu}(^3P_0), \quad (20b)$$

$$\Delta\bar{\nu}_3=\{4.10+0.30[p_0(63,T)+1]+0.20[p_0(19,T)+1]+0.50p_0(77,T)+50(T/\theta_D)^7\xi_6(\theta_D/T)\}\text{cm}^{-1}-\Delta\bar{\nu}(^3P_0). \quad (20c)$$

The first term in Eqs. (20a)–(20c), is the temperature-independent multiphonon relaxation coefficient $\sum_{j<i}K_{ij}$ discussed in Sec. V-A. The interesting feature of these relations is the fact that the Raman coefficients $\bar{\alpha}_i$ are down nearly an order of magnitude from those encountered in the $^3H_4$ and $^3H_6$ manifolds. This will allow us to make an estimate of the $^3P_0$ contribution to transition linewidths.

Results of the linewidth measurements for the $^3P_0\rightarrow{}^3F_4$ transitions are shown in Fig. 13. We did not attempt to obtain a curve fit for these widths, since the lines are not well resolved, and the positions of the energy levels of the $^3F_4$ manifold (Fig. 8) are such as to make the process difficult.

(iv) Widths of the $^3P_0$ State

The temperature dependence of the width of the $^3P_0$ state is given by Eq. (11). Without *a priori* knowledge of the crystal-field parameters entering into the D operator, a precise separation of the $^3P_0$ contribution in Eqs. (18a)–(18c), (19a), (19b), and (20a)–(20c) is impossible. Equation (20a), however, puts an upper limit to the broadening of the $^3P_0$ state, since

$$\bar{\alpha}(^3P_0)\leq\bar{\alpha}(^3F_2)_1=30\text{ cm}^{-1}.$$

Thus,

$$\Delta\bar{\nu}(^3P_0)_{\text{MAX}}=30(T/\theta_D)^7\xi_6(\theta_D/T), \quad (21)$$

which at 300°K yields a value of $\sim$4.0 cm^{-1}. Hence, for the $(^3H_4)$ and $(^3H_6)$ levels studied, the maximum contribution possible to the linewidth due to the broadening of the $^3P_0$ state is never larger than 20%, and Eqs. (18) and (19) represent the actual widths of the levels to within this accuracy.

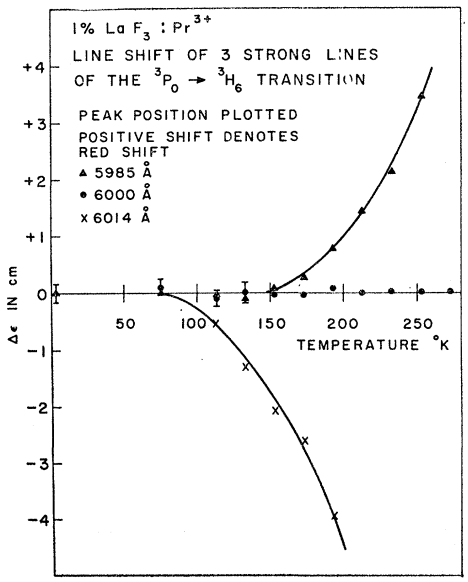

FIG. 15. Peak positions of three strong lines of the $^3P_0\rightarrow{}^3H_6$ transition plotted against temperature. Line pulling accounts for the observed peak shifts.

C. Line Shifts

The positions of the transitions $^3P_0 \rightarrow {}^3F_4$, $^3F_2$, and $^3H_6$ and $^3H_4 \rightarrow {}^3P_0$ were also investigated as a function of temperature. Results of our measurements are shown in Figs. 14–17.

Figure 14 shows the temperature dependence of the position of the $^3P_0$ state inferred from the $^3H_4 \rightarrow {}^3P_0$ measurements and where we have used the ground state, i.e., the $(^3H_4)_1$ level, as the zero reference point. From Eq. (18), it should be clear that the ground state need not be stationary. At higher temperatures, the position of the $(^3H_4)_1 \rightarrow {}^3P_0$ is difficult to measure with great accuracy, due to the considerable broadening of the transition widths, and the results above 200°K should be taken as minimum shift values of the $^3P_0$ state.

No attempt was made to correlate the observed values quantitatively, although correlation is possible; we can, however, point out some qualitative features of the energy shift of rare-earth ions in crystals.

The position shifts of the peaks of the 5985 Å and 6014 Å lines of the $^3P_0 \rightarrow {}^3H_6$ manifold (Fig. 15) may be accounted for by line pulling due to thermal broadening of the three lines studied[35]; thus, the $(^3H_6)_{1,2,3}$ levels appear to shift with the same thermal dependence as the $^3P_0$ state. For the transitions involving the $^3F_2$ and $^3F_4$ states (Figs. 16 and 17), again using the $(^3H_4)_1$ position as the zero-energy reference point, correction for the temperature dependence of the $^3P_0$ position

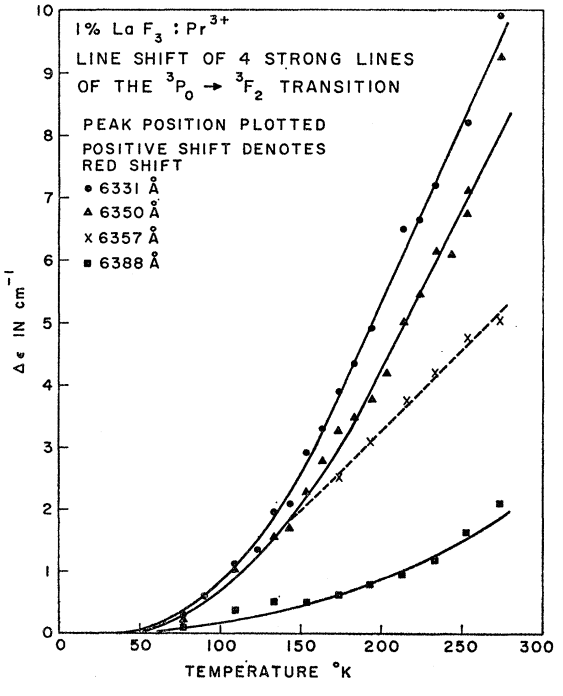

FIG. 16. Peak positions of $^3P_0 \rightarrow {}^3F_2$ transitions as a function of temperature. $^3F_2$ level shifts are obtained by correcting for $^3P_0$ shift given by Fig. 14.

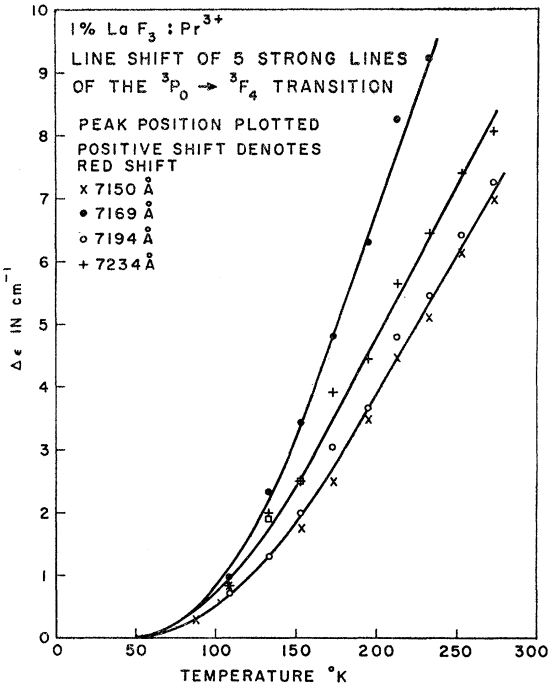

FIG. 17. Peak positions of $^3P_0 \rightarrow {}^3F_4$ transitions versus temperature.

yields level shifts in these manifolds to the red as well as to the blue. Shifts of this nature have been reported by Paetzold in levels of Nd^{3+} in hydrated salts and cannot be accounted for by thermal changes in the lattice parameters.[2,9]

Consideration of the shift expression [Eq. (8)], yields a tentative explanation. From Eqs. (6a) and (6b), the linewidth Raman coeficient $\bar{\alpha}_i$ is roughly the square of the line shift coefficient $\bar{\alpha}_i$ in Eq. (8); for the $^3F_2$ manifold, from Eqs. (20a)–(20c), the Raman coefficient is small implying that α_i will also be small. Conceivably, in cases like this, the contributions from the principal part integrals might be comparable to those from the first term of Eq. (8); if this is the case, the shift for $(^3F_2)_1$ will be unidirectional with the α_i term since all nearby crystal-field levels are such that $j>i$, whereas, for $(^3F_2)_4$, with $j<i$, the principal part contribution will be in a direction opposite to the α_i term. That this is the case is easily verified from Fig. 6.

VI. DISCUSSION

By consideration of a simple phonon-ion interaction picture, we have shown that this model accounts adequately for the temperature dependence of the linewidths and possibly the positions of optical transitions of $LaF_3:Pr^{3+}$.

Since crystal fields can be considered as perturbations in the case of $4f$ electrons, the rare earths lend themselves nicely to theoretical calculation. Thus, in principle, by using the methods of Elliott and Stevens,[18,19]

it would be possible to evaluate the crystal-field matrix elements due to perturbations C and D.[48] Unfortunately, the low symmetry and the complete lack of knowledge of crystalline-field parameters of the ion site of Pr^{3+} in LaF_3 prevent us from other than a semiempirical determination of the matrix elements appearing in Eq. (7). It would be of considerable interest to extend this study to rare-earth ions in crystal lattices where there exists more knowledge of crystalline-field parameters and the site symmetries may be analyzed with less tedium.

With the aid of knowledge of the effective density of phonon states and from the direct process coefficients β_{ij}, we may determine the relative sizes of the matrix elements of operator C. For example, from values obtained in Sec. V-B, and referring to Fig. 4, for the $(^3H_6)$ states

$$|\langle(^3H_6)_3|C|(^3H_6)_1\rangle|^2\cong 0.67|\langle(^3H_6)_2|C|(^3H_6)_1\rangle|^2 \quad (22a)$$

and

$$|\langle(^3H_6)_3|C|(^3H_6)_2\rangle|^2\cong 1.40|\langle(^3H_6)_2|C|(^3H_6)_1\rangle|^2. \quad (22b)$$

Equations of the type (22a) and (22b), which may be obtained semiempirically, should serve as a considerable time-saving aid in the calculation of crystalline-field perturbations.

It is also interesting to point out that correlation may now be obtained between optical linewidth studies and ESR spin-lattice relaxation measurements. In fact, the so-called Orbach process[28,49,50] in ESR which normally involves the first excited state of the ground-state manifold yields a coefficient which is just the direct process coefficient between the first excited and the ground states. As it has already been pointed out, the magnitude of this coefficient leads to observable broadening of the excited level. In the case of Pr^{3+} in LaF_3, the C_{2v} coordination of the ion site lifts all degeneracy and no ESR studies are possible on the ground state. Correlation in this coordination is, however, possible in Kramers degenerate ions and are now being conducted in this laboratory.[51]

A more detailed quantitative study need be made of the temperature dependence of the level positions of rare-earth ions in solids. Confirmation of Eq. (8) would yield additional information on the lattice-ion interaction parameters C and D; such a study is now also being conducted in this laboratory on $LaF_3:Nd^{3+}$.[52]

Linewidth studies as a function of concentration of impurity ions should also be conducted to ascertain the effect of exchange and other phonon-related phenomena.

ACKNOWLEDGMENTS

We would like to thank H. Muir and R. Solomon of Varian Associates, Palo Alto, for providing us with the necessary samples, and H. G. Freie for experimental assistance. It is with pleasure that we acknowledge numerous fruitful discussions with G. Frank Imbusch and Professor P. L. Scott; their critical reading of this manuscript is also greatly appreciated. One of us (WMY) would like to acknowledge cooperation and support from Varian Associates, Crystal and Central Research Department, Palo Alto. The high-resolution scanning spectrometer was made available to us by the Advanced Research Projects Agency, through the Center for Materials Research at Stanford University.

[48] Contributions from the C operator may also be evaluated empirically by the use of the stress method of Ref. 32.

[49] R. Orbach, Proc. Roy. Soc. (London) A264, 456 (1961).

[50] C. B. P. Finn, R. Orbach, and W. P. Wolf, Proc. Phys. Soc. (London) 77, 261 (1961).

[51] The 4.2°K, $^4S_{3/2}\rightarrow{}^4I_{15/2}$ transition of $LaF_3:Er^{3+}$ is such a possibility. The spectrum of Er^{3+} in LaF_3 has been published: W. F. Krupke and J. B. Gruber, J. Chem. Phys. 39, 1024 (1963).

[52] H. G. Freie, W. M. Yen, and A. L. Schawlow (to be published).

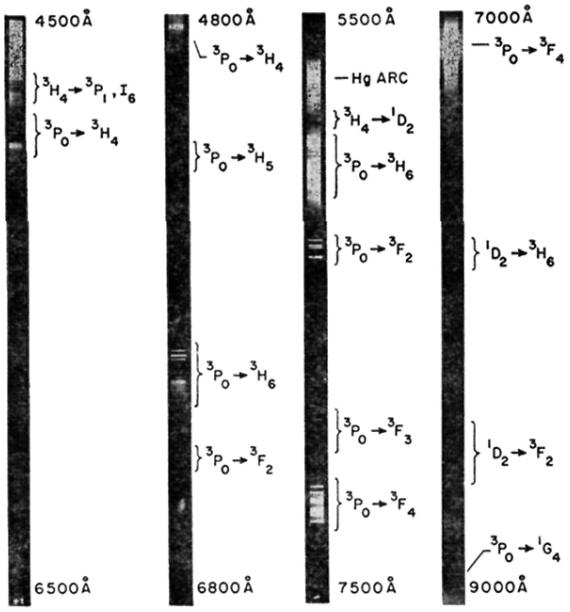

FIG. 2. Optical spectrum of 1% $LaF_3:Pr^{3+}$ at 77°K. Transitions involved are as shown; very sharp lines are gas discharge references.